Structural Phase Transitions in $A_{2-x}Sr_xNiWO_6$ (A = Ca or Ba, $0 \leq x \leq 2$) Double Perovskites

Qingdi Zhou,[†] Brendan J. Kennedy,*[,†] Christopher J. Howard,[‡] Margaret M. Elcombe,[§] and Andrew J. Studer[§]

School of Chemistry, The University of Sydney, Sydney, New South Wales 2006, Australia, Institute of Materials and Engineering Science, ANSTO, Private Mail Bag 1, Menai, New South Wales 2334, Australia, and Bragg Institute, ANSTO, Private Mail Bag 1, Menai, New South Wales 2234, Australia

Received April 28, 2005. Revised Manuscript Received July 29, 2005

Twenty-seven samples in the series of mixed double perovskites of the type A_2NiWO_6 where A is a suitable alkaline earth cation or combination of such cations (Ca, Ca with Sr, Sr, Sr with Ba, or Ba) have been prepared using $NiWO_4$ as a starting material. The structures of the oxides have been determined using synchrotron X-ray powder diffraction methods, with additional neutron patterns being collected for a smaller number of samples. These studies demonstrated the symmetry increases with the average size of the A-site cation (r_A) as follows: $P2_1/n \xrightarrow{r_A = 1.430\ \text{Å}} I4/m \xrightarrow{r_A = 1.480\ \text{Å}} Fm\bar{3}m$. Temperature-dependent structural studies have been undertaken for selected samples.

Introduction

The importance of oxides with the perovskite structure in modern materials continues to grow with such oxides finding applications in diverse fields including ferroelectrics, high-temperature superconductors, materials exhibiting colossal magnetoresistive effects, ionic conductors, etc.[1] Perovskite oxides with ABO_3 stoichiometry have a structure based on a three-dimensional framework of corner-sharing BO_6 octahedra, with the A-type cation occupying the resulting high-coordination sites. Very few perovskites have the archetypal cubic structure, rather a number of lower symmetry variants exist as a result of the ability of the corner-sharing octahedral framework to undergo cooperative tilting distortions. Octahedral tilting occurs as a consequence of the mismatch in size between the A-site cation and the corner-sharing octahedral network.[2] Phase transitions between various ABO_3 perovskite structures with different tilt patterns have been extensively studied.[1,3] The propensity of oxides to adopt the perovskite structures allows chemical substitutions to be made on both cation sites as well as on the anion site. Where two different ions occupy the octahedral site in approximately equal amounts, ordering of these cations is common, and the resulting $A_2BB'O_6$ oxides are referred to as double perovskites.[4]

The recent discovery of the room temperature magnetoresistance in $A_2BB'O_6$ (A is an alkaline earth; B and B′ are heterovalent transition metals) double perovskites has generated immense interest in these materials because of their potential importance as magnetotransport devices as well as their rich and challenging properties.[5−9] The structural and magnetic properties of B-site ordered double perovskite oxides can be tuned by changing either the number of d-electrons of the B-site cation and/or the size of the cations. These substitutions can result in significant structural distortions. These structural distortions are therefore not only interesting crystallographically, but they are also important since the distortions can have critical influence on the electric and magnetic properties of the perovskite material.[10,11]

The oxides A_2NiWO_6 (A = Ca, Sr, Ba) have been known for some time and are examples of ordered double perovskites.[1] These oxides illustrate the role of the size of the A cation in influencing the precise structure of double perovskites. Whereas Ca_2NiWO_6 is monoclinic (space group $P2_1/n$) with both in-phase and out-of-phase tilts of the $(Ni,W)O_6$ octahedra, Sr_2NiWO_6 is tetragonal ($I4/m$) with an out-of-phase tilt only, and Ba_2NiWO_6 is cubic $Fm\bar{3}m$ without tilting. In the present work, we have sought to establish the temperature and composition dependence of the structure

* Corresponding author. E-mail: b.kennedy@chem.usyd.edu.au.
† The University of Sydney.
‡ Institute of Materials and Engineering Science.
§ Bragg Institute.

(1) Mitchell, R. H. *Perovskites: Modern and Ancient*; Almaz Press: Ontario, Canada, 2002.
(2) Glazer, A. M. *Acta Crystallogr., Sect. B* **1972**, *28*, 3384.
(3) Kennedy, B. J.; Howard, C. J.; Chakoumakos, B. C. *J. Phys.: Condens. Matter* **1999**, *11*, 1479−1488.
(4) Anderson, M. T.; Greenwood, K. B.; Taylor, G. A.; Poeppelmeir, K. R. *Prog. Solid State Chem.* **1993**, *22*, 197.
(5) Kobayashi, K. L.; Kimura, T.; Sawada, H.; Terakura, K.; Tokura, Y. *Nature* **1998**, *395*, 677−680.
(6) DeMarco, M.; Blackstead, H. A.; Dow, J. D.; Wu, M. K.; Chen, D. Y.; Chien, E. Z.; Haka, H.; Toorongian, S.; Fridmann, J. *Phys. Rev. B* **2000**, *62*, 14301−14303.
(7) Chmaissem, O.; Kruk, R.; Dabrowski, B.; Brown, D. E.; Xiong, X.; Kolesnik, S.; Jorgensen, J. D.; Kimball, C. W. *Phys. Rev. B* **2000**, *62*, 14197.
(8) Moritomo, Y.; Xu, S.; Machida, A.; Akimoto, T.; Nishibori, E.; Takata, M.; Sakata, M.; Ohoyama, K. *J. Phys. Soc. Jpn.* **2000**, *69*, 1723.
(9) Azad, A. K.; Eriksson, S. G.; Ivanov, S. A.; Mathieu, R.; Svedlindh, P. *Ferroelectrics* **2004**, *302*, 427−431.
(10) Philipp, J. B.; Majewski, P.; Alff, L.; Erb, A.; Gross, R.; Graf, T.; Brandt, M. S.; Simon, J.; Walther, T.; Mader, W.; Topwal, D.; Sarma, D. D. *Phys. Rev., B* **2003**, *68*, 14443.
(11) Popov, G.; Greenblatt, M.; Croft, M. *Phys. Rev., B* **2003**, *67*, 024406.

10.1021/cm050900k CCC: $30.25
Published on Web 09/14/2005

across the full range of A-cation sizes through a study of the family of double perovskites, $A_{2-x}Sr_xNiWO_6$ (A = Ca or Ba, $0 \leq x \leq 2$). In particular, we wish to establish how the structure responds to changes in the effective size of the cation occupying the perovskite A-type site, and we have done this using a combination of high-resolution synchrotron X-ray and neutron powder diffraction methods.

Experimental Section

All starting materials were obtained from Aldrich Chemicals and used without purification. Crystalline samples of $A_{2-x}Sr_xNiWO_6$ (A = Ca, x = 0, 0.1, 0.2, 0.4, 0.5, 0.6, 0.75, 0.8, 1, 1.2, 1.4, 1.5, 1.6, 1.7, 1.8, 2; A = Ba, x = 0, 0.5, 0.75, 1, 1.25, 1.5, 1.6, 1.7, 1.75, 1.8, 1.9) were synthesized using $NiWO_4$ as a precursor. $NiWO_4$ was prepared by conventional solid-state methods from stoichiometric amounts of NiO (99.99% purity) and WO_3 (99.995%). These were mixed and heated at 1000 °C/12 h, 1100 °C/12 h, and 1150 °C/48 h with intermediate regrinding. To make the $A_{2-x}Sr_xNiWO_6$ samples, appropriate amounts of $NiWO_4$ and the required alkaline earth metal carbonate ($BaCO_3$, 99.98%; $CaCO_3$, 99.995%; or $SrCO_3$, 99.9+%) were weighed, mixed in the presence of acetone, and heated at 1000 °C/12 h, at 1100 °C/12 h, and finally at 1150 °C/80 h and with periodic regrinding.

The reactions were followed by powder X-ray diffraction using Cu Kα radiation on a Shimadazu D6000 diffractometer. Synchrotron X-ray diffraction data for the final samples were recorded on the Debye Scherrer diffractometer at the Australian National Beamline Facility, Beamline 20B at the Photon Factory, Tsukuba, Japan.[12] The samples were housed in 0.3 mm diameter capillaries that were rotated during the measurements. Data were collected using two image plates as detectors covering the angular range $5 < 2\theta < 85°$, step size 0.01° using X-rays of wavelength 0.8028(1) Å. The image plates were scanned at a 100 μm resolution, which corresponds to 0.01°degrees for the camera radius of 573 mm.

The minimum observed full width at half-maximum height in patterns from these samples was $\Gamma_{min} \sim 0.035°$. Variable temperature data were collected, using a custom-built furnace, at temperatures of up to 800 °C.

Neutron powder diffraction data for selected samples were collected at room temperature with the high-resolution powder diffractometer (HRPD)[13] at the Australian research reactor, HIFAR (λ = 1.4924(1) Å, $10 < 2\theta < 150°$, step size 0.05°, $\Gamma_{min} \sim 0.35°$). The samples were held in vanadium containers. Variable temperature neutron diffraction patterns were recorded for a sample of Sr_2NiWO_6 using the medium resolution powder diffractometer (MRPD)[14] at the same facility (λ = 1.6646(1) Å, $10 < 2\theta < 138°$, step size 0.1°, $\Gamma_{min} \sim 0.45°$). For these measurements, the sample was housed in a stainless steel can that was open to the atmosphere.

Refinements of the crystal structures were performed with program RIETICA.[15] The diffraction peaks were described by a pseudo-Voigt function where the Lorentzian fraction is refined. For the neutron diffraction studies, a correction for peak asymmetry was applied. The background was described by a six-parameter polynomial. For the X-ray patterns, the background was estimated by interpolation between up to 40 user selected points. During the refinements, the occupancies of the two octahedrally coordinated metal cations (Ni and W) were allowed to vary over the two possible metal sites; however no anti-site disorder was observed. Consequently in the final refinement cycles the occupancies were fixed.

Results and Discussion

To achieve the range of structures from monoclinic in $P2_1/n$ to cubic in $Fm\bar{3}m$, it was necessary to prepare two series of oxides, $Ca_{2-x}Sr_xNiWO_6$ and $Ba_{2-x}Sr_xNiWO_6$. These series cover the range of fitness factors, as described by Teraoka et al.,[16] from 0.926 to1.113 as the effective ionic radii of the A-site cation increases from 1.34 to 1.61 Å. In general, fitness factor values greater than 1.00 are expected to result in a cubic lattice, while values less than 0.9 are expected to result in a monoclinic lattice in $P2_1/n$. We note from Table 1 that the tolerance factor appears to be a better indication of transition from cubic symmetry. Although the apparent coordination of the A-type cation changes as the symmetry is lowered, we have used the tabulated ionic radii for 12-fold coordination of these cations to estimate the tolerance factor and measure of fit. The strategy of preparing two series of solid solutions to span the range of expected structures has been used recently by Mountstevens et al.[17] in the study of some tin perovskites and by Chmaissem et al. for manganese perovskites.[18]

Synthesis. Pure samples of $A_{2-x}Sr_xNiWO_6$, 27 samples in all, were successfully prepared. All were pale green in color and highly crystalline. The use of $NiWO_4$ as precursor ensured that there were no contaminant secondary phases, such as $SrWO_4$ or Sr_2WO_5, in the final product.

Room Temperature Structures. The results from our structural studies are summarized in Table 1, and the composition dependence of the lattice parameters is illustrated in Figure 1. The diffraction pattern of Ba_2NiWO_6 was undoubtedly that of a cubic material with a = 8.0703(1) Å. The presence of a strong 111 reflection near d = 4.58 Å showed the Ni and W cations to be ordered, and the structure was refined in the cubic space group $Fm\bar{3}m$. No splitting or asymmetry of any of the reflections was observed in the series $Ba_{2-x}Sr_xNiWO_6$ for x from 0 to 1.5, the volume of the cell reducing as the Sr content increased (Figure 2). At x = 1.6, that is for $Ba_{0.4}Sr_{1.6}NiWO_6$, slight asymmetry was observed for a number of the high angle reflections, and the pattern was better fitted in the tetragonal space group $I4/m$. Ultimately the pattern of the sample at x = 1.5 was also fitted in this space group. The absence of any M-point reflections indicative of in-phase rotation of the BO_6 octahedra is consistent with this choice.[19] As the Sr content was further increased, the asymmetry of the diagnostic reflections progressively increased until the overlapping lines were well-separated, indicative of increasing tetragonal distortion (Figures 1 and 3). The structure of Sr_2NiWO_6 has

(12) Sabine, T. M.; Kennedy, B. J.; Garrett, R. F.; Foran, G. J.; Cookson, D. J. *J. Appl. Crystallogr.* **1995**, *28*, 513.
(13) Howard, C. J.; Ball, C. J.; Davis, R. L.; Elcombe, M. M. *Aust. J. Phys.* **1983**, *36*, 507.
(14) Kennedy, S. J. *Adv. X-Ray Anal.* **1995**, *38*, 35.
(15) Howard, C. J.; Hunter, B. A. *A Computer Program for Rietveld Analysis of X-ray and Neutron Powder Diffraction Patterns*; Lucas Heights Research Laboratories: NSW, Australia, 1998; pp 1−27.
(16) Teraoka, Y.; Wei, M. D.; Kagawa, S. *J. Mater. Chem.* **1998**, *8*, 2323−2325.
(17) Mountstevens, E. H.; Attfield, J. P.; Redfern, S. A. T. *J. Phys.-Condens. Matter* **2003**, *15*, 8315−8326.
(18) Chmaissem, O.; Dabrowski, B.; Kolesnik, S.; Mais, J.; Brown, D. E.; Kruk, R.; Prior, P.; Pyles, B.; Jorgensen, J. D. *Phys. Rev., B* **2001**, *64*, 134412.
(19) Howard, C. J.; Kennedy, B. J.; Woodward, P. M. *Acta Crystallogr., Sect. B* **2003**, *B59*, 463.

Table 1. Refined Cell Parameters, Unit Cell Volume, and Space Group for the Series A_2NiWO_6 at Room Temperature[a]

compound	A cation size (Å)[b]	t[c]	fitness[d]	a (Å)	b (Å)	c (Å)	β (°)	unit cell vol (Å^3)	space group
Ca_2NiWO_6	1.34	0.947	0.927	5.4021(1)	5.5351(1)	7.6862(1)	90.241(1)	229.82(1)	$P2_1/n$
$Ca_{1.9}Sr_{0.1}NiWO_6$	1.345	0.949	0.930	5.4153(1)	5.5371(1)	7.7012(1)	90.202(1)	230.92(1)	$P2_1/n$
$Ca_{1.8}Sr_{0.2}NiWO_6$	1.35	0.951	0.934	5.4305(2)	5.5404(2)	7.7183(2	90.164(2)	232.22(1)	$P2_1/n$
$Ca_{1.6}Sr_{0.4}NiWO_6$	1.36	0.954	0.941	5.4519(1)	5.5350(1)	7.7403(1)	90.117(2)	233.57(1)	$P2_1/n$
$Ca_{1.5}Sr_{0.5}NiWO_6$	1.365	0.956	0.944	5.4642(2)	5.5275(2)	7.7552(3)	90.208(3)	234.23(1)	$P2_1/n$
$Ca_{1.4}Sr_{0.6}NiWO_6$[e]	1.37	0.958	0.947	5.4727(1)	5.5254(1)	7.7605(2)	90.073(6)	234.67(1)	$P2_1/n$
$Ca_{1.25}Sr_{0.75}NiWO_6$[e]	1.3775	0.960	0.953	5.4912(2)	5.5225(2)	7.7785(3)	90.093(6)	235.88(1)	$P2_1/n$
$Ca_{1.2}Sr_{0.8}NiWO_6$	1.38	0.961	0.954	5.4981(2)	5.5306(2)	7.7883(2)	90.033(15)	236.83(1)	$P2_1/n$
$CaSrNiWO_6$	1.39	0.965	0.961	5.5200(3)	5.5195(3)	7.8134(3)	90.166(3)	238.06(2)	$P2_1/n$
$Ca_{0.8}Sr_{1.2}NiWO_6$	1.4	0.968	0.968	5.5320(1)	5.5319(1)	7.8233(1)	90.113(1)	239.40(1)	$P2_1/n$
$Ca_{0.6}Sr_{1.4}NiWO_6$	1.41	0.972	0.975	5.5439(2)	5.5454(3)	7.8359(2)	90.007(5)	240.90(1)	$P2_1/n$
$Ca_{0.5}Sr_{1.5}NiWO_6$	1.415	0.973	0.979	5.5454(1)	5.5517(2)	7.8426(3)	90.015(3)	241.45(1)	$P2_1/n$
$Ca_{0.4}Sr_{1.6}NiWO_6$	1.42	0.975	0.982	5.5488(1)	5.5603(1)	7.8471(1)	90.009(6)	242.10(1)	$P2_1/n$
$Ca_{0.3}Sr_{1.7}NiWO_6$	1.425	0.977	0.985	5.5505(1)	5.5679(1)	7.8506(1)	90.010(4)	242.62(1)	$P2_1/n$
$Ca_{0.2}Sr_{1.8}NiWO_6$	1.43	0.979	0.989	5.5567(1)	5.5764(1)	7.8582(1)	90.007(6)	243.50(1)	$P2_1/n$
Sr_2NiWO_6	1.44	0.982	0.996	5.5613(1)		7.9185(1)		244.91(1)	$I4/m$
$Ba_{0.1}Sr_{1.9}NiWO_6$	1.4485	0.985	1.002	5.5699(1)		7.9204(1)		245.72(1)	$I4/m$
$Ba_{0.2}Sr_{1.8}NiWO_6$	1.457	0.988	1.008	5.5793(1)		7.9217(1)		246.59(1)	$I4/m$
$Ba_{0.25}Sr_{1.75}NiWO_6$	1.46125	0.989	1.011	5.5840(1)		7.9203(1)		246.96(1)	$I4/m$
$Ba_{0.3}Sr_{1.7}NiWO_6$	1.4655	0.991	1.013	5.5909(1)		7.9260(1)		247.75(1)	$I4/m$
$Ba_{0.4}Sr_{1.6}NiWO_6$	1.474	0.994	1.019	5.6015(1)		7.9288(1)		248.78(1)	$I4/m$
$Ba_{0.5}Sr_{1.5}NiWO_6$	1.4825	0.997	1.025	5.6099(1)		7.9353(3)		249.73(1)	$I4/m$
$Ba_{0.75}Sr_{1.25}NiWO_6$	1.50375	1.004	1.040	7.9578(1)				503.94(1)	$Fm3m$
$BaSrNiWO_6$	1.525	1.011	1.055	7.9803(1)				508.22(1)	$Fm3m$
$Ba_{1.25}Sr_{0.75}NiWO_6$	1.54625	1.019	1.069	8.0002(1)				512.03(1)	$Fm3m$
$Ba_{1.5}Sr_{0.5}NiWO_6$	1.5675	1.026	1.084	8.0242(1)				516.67(1)	$Fm3m$
Ba_2NiWO_6	1.61	1.041	1.113	8.0703(1)				525.62(1)	$Fm3m$

[a] The numbers in parentheses are the estimated standard deviations. [b] Weighted average assuming 12-fold coordination environment of the A-type cation. [c] Tolerance factor given by $t = \frac{r_A + r_O}{\sqrt{2}(r_B + r_O)}$. [d] Measure of fit given by $t = \frac{\sqrt{2}r_A}{(r_B + r_O)}$. [e] Values obtained using data collected on a conventional diffractometer.

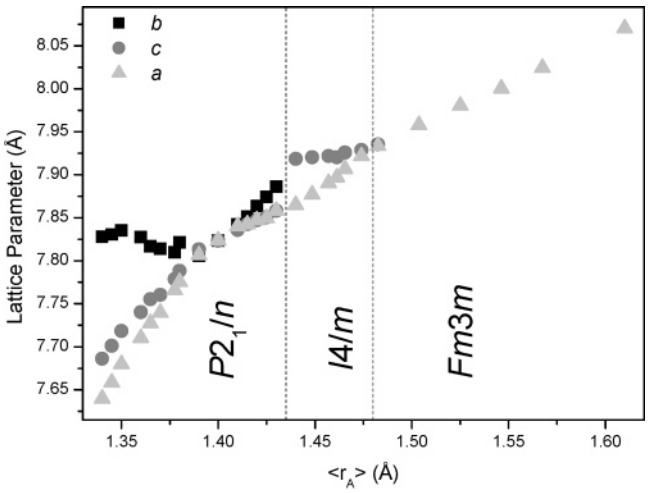

Figure 1. Variation of the reduced lattice parameters with the average A cation radius for the series A_2NiWO_6. The vertical lines show the approximate transitions between the three observed structural types. The a and b values in the monoclinic and tetragonal cells have been multiplied by $\sqrt{2}$ for clarity. The estimated errors in the values are smaller than the symbol sizes.

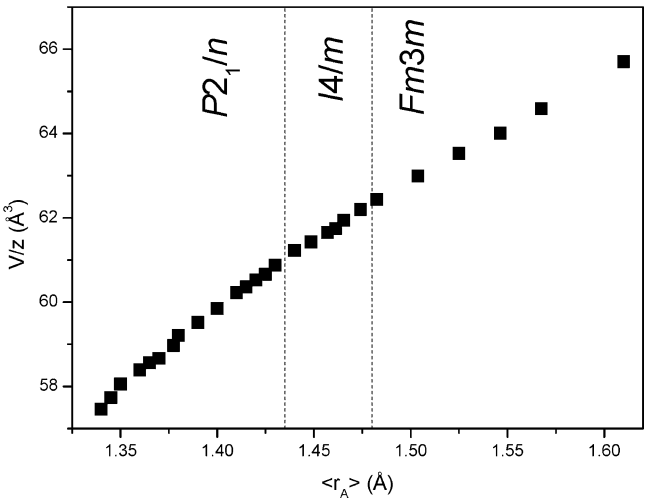

Figure 2. Variation of the volume/Z with average A cation radius in the series A_2NiWO_6. The estimated errors in the values are smaller than the symbol sizes.

been refined in the tetragonal space group $I4/m$ previously,[20] and our results are in good agreement with those from that work.

In the solid solutions $Ca_{2-x}Sr_xNiWO_6$ we observe a remarkable and dramatic simplification of the diffraction pattern at $x = 1.8$. The pattern of this material appears cubic although a number of reflections are noticeably broader than expected for a cubic material. Although the pattern could be fitted in a tetragonal model in $I4/m$, it required a significant change in the tetragonal c/a ratio from that observed in Sr_2NiWO_6 (see Figure 1). We infer that there has been a first order change from the structure in $I4/m$ ($a^0a^0c^-$) to either a structure in $I2/m$ ($a^0b^-b^-$) or the most commonly observed[21] double perovskite structure in space group $P2_1/n$ ($a^+b^-b^-$). The first transition is analogous to the $I4/mcm$ to $Imma$ transition observed in a number of simple ABO_3 perovskites[22,23] and has been observed in

(20) Gateshki, M.; Igartua, J. M.; Hernandez-Bocanegra, E. *J. Phys.-Condens. Matter* **2003**, *15*, 6199−6217.

(21) Woodward, P. M. *Acta Crystallogr., Sect. B* **1997**, *53*, 44.

(22) Howard, C. J.; Knight, K. S.; Kennedy, B. J.; Kisi, E. H. *J. Phys.-Condens. Matter* **2000**, *12*, L677−L683.

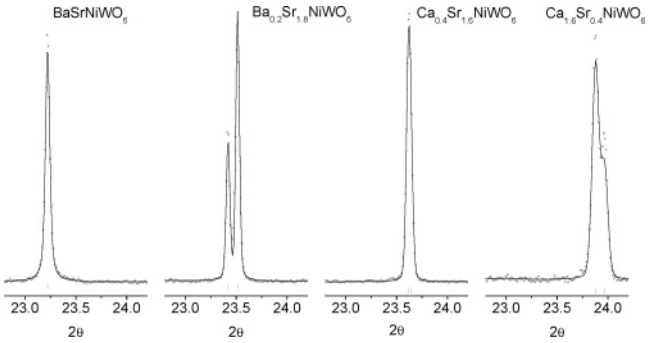

Figure 3. Portions of the observed and calculated powder X-ray diffraction profiles for four members in the series A_2NiWO_6. The space group alters from $Fm\bar{3}m$ in $BaSrNiWO_6$ to $I4/m$ in $Ba_{0.2}Sr_{1.8}NiWO_6$ and $P2_1/n$ in $Ca_{0.4}Sr_{1.6}NiWO_6$ and $Ca_{1.6}Sr_{0.4}NiWO_6$. The progressive increase in angle is a consequence of the decrease in size of the A-site cation.

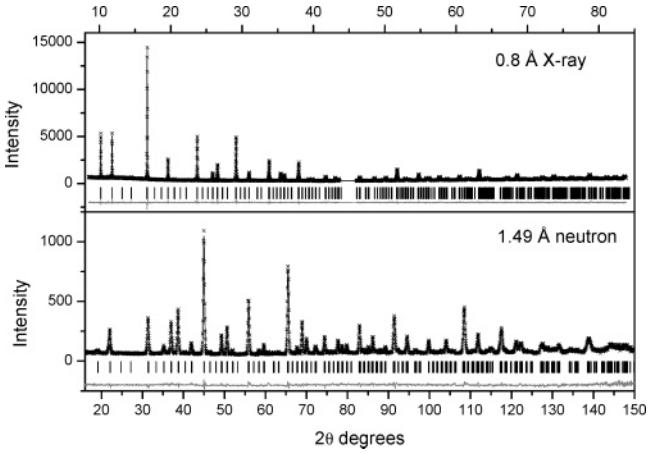

Figure 4. Observed, calculated, and difference profiles for $CaSrNiWO_6$. The upper trace shows the X-ray diffraction profile from 10 to 80° (top axis) whereas the lower trace shows the neutron diffraction profile from 15 to 150°. The gap near 45° in the X-ray data is from the gap between the image plates.

variable temperature X-ray diffraction studies of Sr_2MnTeO_6[24] as well as in a small number of fluorides such as Cs_2RbDyF_6.[25] Structural models in $I2/m$ and $P2_1/n$ gave comparable fits to the data. The presence of *M*-point reflections, indicative of in-phase (+) tilting, would establish the structure as that in $P2_1/n$. No such reflections were seen in the X-ray pattern, but since these are expected to be very weak, it is not possible to distinguish between the two space groups from X-ray diffraction data alone. Neutron diffraction patterns, however, at $x = 1.7$ and below ($Ca_{0.3}$ and above) showed *M*-point reflections, so for these compositions the structure was shown to be that in $P2_1/n$ (see below).

As the Ca content further increased to around $x = 1.2$ the appearance of the X-ray diffraction patterns remained simple, and these were all well fitted in $P2_1/n$. At still higher Ca contents, the complexity of the patterns rapidly increased and the structure was clearly monoclinic (Figure 1).

The synchrotron X-ray diffraction pattern for Ca_2NiWO_6 showed a number of weak *M*-point and *X*-point reflections indicating in-phase or + tilts of the BO_6 octahedra are present. In this case it is apparent even from the X-ray data that space group $P2_1/n$ ($a^+b^-b^-$) is appropriate.

Despite the first-order monoclinic to tetragonal transition occurring near $r_A = 1.43$ Å, there is no apparent discontinuity in the volume as the composition is altered. Indeed it is only at very high Ca contents that a noticeable variation from Vegard's law (linear dependence of volume on size) is observed (Figure 2), and this is believed to be a result of strains induced by tilting of the BO_6 octahedra.[26,27]

The X-ray data show that there is a first-order $I4/m$ to monoclinic transition; however, they cannot easily establish if the transition proceeds directly to $P2_1/n$ or goes via an $I2/m$ intermediate. Distinguishing these possibilities requires identification of the symmetry and tilt system, and that in turn requires analysis of the superlattice reflections. Neutron diffraction methods were used in order to distinguish between the two proposed monoclinic structures. Neutron methods are less sensitive than X-ray methods to the cation ordering but are considerably more sensitive to the displacement of the oxygen anions that occurs as a consequence of tilting of the BO_6 octahedra. These differences are evident in Figure 4. Neutron patterns were collected at room temperature using the HRPD for three samples, namely, $CaSrNiWO_6$, $Ca_{0.5}Sr_{1.5}NiWO_6$, and $Ca_{0.3}Sr_{1.7}NiWO_6$ corresponding to $r_A = 1.39$, 1.415, and 1.425 Å. As noted earlier, neutron data were recorded from Sr_2NiWO_6, $r_A = 1.44$ Å, using MRPD, and the structure was shown to be tetragonal. This tetragonal structure is observed in a number of related oxides with similar tolerance factors including Sr_2NiMoO_6, Sr_2CoWO_6, and Sr_2MnWO_6.[28−30]

The neutron diffraction pattern for $CaSrNiWO_6$ showed strong *M*-point reflections indicative of in-phase BO_6 tilting. The strongest of these reflections, those that fall near $2\theta = 35$ and 42° (for $\lambda = 1.49$ Å), are included in the extracts shown in Figure 5. Increasing the Sr content reduces the magnitude of the distortion but more importantly decreases the strength of the *M*-point superlattice reflections. This corresponds to a reduction in the tilts. The magnitudes of the tilts were estimated from the refined atomic coordinates. For $CaSrNiWO_6$, we observe relatively large in-phase and out-of-phase tilts around each metal center with $\theta \approx 9.6$ and 10.5° and $\varphi \approx 7.7$ and 8.1° for the W and Ni, respectively. Increasing the Sr content to $Ca_{0.5}Sr_{1.5}NiWO_6$ results in a reduction in the magnitude of the tilts to $\theta \approx 2°$ around both Ni and W and $\varphi \approx 0.1°$.[31] The observed intensity associated with the *M*-points shows these are not zero. Indeed we estimate from the trend that the *M*-point reflections would remain even at $Ca_{0.2}Sr_{1.8}NiWO_6$; hence, we conclude that

(23) Kennedy, B. J.; Hunter, B. A.; Hester, J. R. *Phys. Rev., B* **2002**, *65*, 224103.
(24) Ortega-San Martin, L.; Chapman, J. P.; Hernández-Bocanegra, E.; Insausti, M.; Arriortua, M. I.; Rojo, T. *J. Phys.,-Condens. Matter* **2004**, *16*, 3879−3888.
(25) Flerov, I. N.; Gorev, M. V.; Aleksandrov, K. S.; Tressaud, A.; Grannec Couzi, M. *Mater. Sci. Eng.* **1998**, *R24*, 81−151.
(26) Carpenter, M. A. *Rev. Mineral. Geochem.* **2000**, *39*, 35−64.
(27) Carpenter, M. A.; Salje, E. K. H.; Graeme-Barber, A. *Eur. J. Mineral.* **1998**, *10*, 621.
(28) Martinez-Lope, M. J.; Alonso, J. A.; Casais, M. T. *Eur. J. Inorg. Chem.* **2003**, *15*, 2839−2844.
(29) Viola, M. C.; Martinez-Lope, M. J.; Alonso, J. A.; Martinez, J. L.; De Paoli, J. M.; Pagola, S.; Pedregosa, J. C.; Fernandez-Diaz, M. T.; Carbonio, R. E. *Chem. Mater.* **2003**, *15*, 1655−1663.
(30) Lin, Q.; Greeenblatt, M.; Croft, M. *J. Solid State Chem.* **2005**, *178*, 1356−66.
(31) Groen, W. A.; Van Berkel, F. P. F.; Ijdo, D. J. W. *Acta Crystallogr., Sect. B* **1986**, *42*, 1472−1475.

Table 2. Structural Parameters for Representative Members of the Series A_2NiWO_6 at Room Temperature[a]

compounds		CaSr*	$Ca_{0.5}Sr_{1.5}$*	$Ca_{0.3}Sr_{1.7}$*	Sr_2	BaSr
space group		$P2_1/n$	$P2_1/n$	$P2_1/n$	$I4/m$	$Fm\bar{3}m$
A	x	0.5093(13)	0.4989(19)	0.5007(7)	0	0.25
	y	0.0263(6)	0.0124(9)	0.0104(5)	0.5	0.25
	z	0.2507(21)	0.2484(24)	0.2498(9)	0.25	0.25
	Biso	0.84(4)	0.94(5)	0.69(2)	1.13(3)	0.54(4)
Ni	x	0	0	0	0	0.5
	y	0	0	0	0	0.5
	z	0	0	0	0.5	0.5
	Biso	0.54(6)	0.67(1)	0.67(1)	0.46(2)	0.26(2)
W	x	0	0	0	0	0
	y	0	0	0	0	0
	z	0.5	0.5	0.5	0	0.
	Biso	0.08(10)	0.67(1)	0.67(1)	0.46(2)	0.26(2)
O1	x	0.2961(13)	0.2797(17)	0.2768(8)	0.2058(18)	0
	y	0.2241(15)	0.2317(21)	0.2360(11)	0.2631(18)	0
	z	−0.0333(12)	−0.0356(11)	−0.0295(6)	0	0.2370(8)
	Biso	1.04(14)	0.67(20)	0.78(11)	0.87(13)	0.80(9)
O2	x	0.2264(12)	0.2279(22)	0.2389(11)	0	
	y	0.7082(17)	0.7116(17)	0.7222(1)	0	
	z	−0.0311(13)	−0.0272(11)	−0.0220(7)	0.2360(13)	
	Biso	0.97(14)	1.48(19)	0.86(10)	0.87(13)	
O3	x	0.4375(11)	0.4607(14	0.4571(5)		
	y	0.4899(8)	0.4947(13)	0.4958(7)		
	z	0.2444(12)	0.2403(15)	0.2420(10)		
	Biso	0.71(7)	0.52(9)	0.71(6)		
R_w		5.34	5.55	4.66	5.77	5.24
R_{wp}		6.44	6.91	6.23	7.31	6.80

[a] In all cases the cations on the A-site were constrained to have equal displacement parameters. An asterisk (*) indicates that refinement used powder neutron diffraction data.

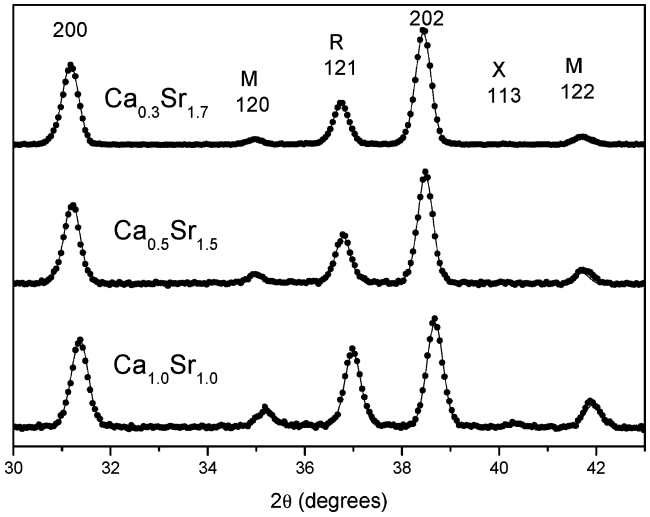

Figure 5. Portions of the neutron diffraction patterns for three samples showing the presence of both *R*- and *M*-point reflections.

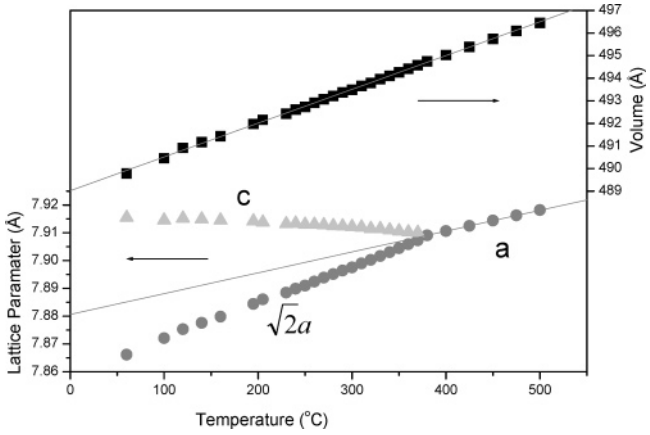

Figure 6. Temperature dependence of the lattice parameters and cell volume for Sr_2NiWO_6. The solid lines are linear fits. For the volume the fit is over the entire temperature range and highlights the absence of any appreciable volume change associated with the phase transition. For the cell parameters, the fit considered only the values in the cubic phase and was extrapolated to the tetragonal region. The estimated errors in the values are smaller than the symbol sizes.

the transformation proceeds from tetragonal $I4/m$ to monoclinic $P2_1/n$ directly.

In summary we have shown the following sequence of phases to exist in the series A_2NiWO_6: A = Ca, Sr, Ba; $P2_1/n \xrightarrow{r_A = 1.430\ \text{Å}} I4/m \xrightarrow{r_A = 1.480\ \text{Å}} Fm\bar{3}m$ with the critical compositions as indicated in Table 2. These correspond to the changes in the tilts as $a^-\ a^-\ c^+ \rightarrow a^0a^0c^- \rightarrow a^0a^0a^0$. This sequence of tilts differs somewhat from that observed in a number of simple ABO_3 perovskites including $SrZrO_3$[22] and $SrRuO_3$[23] as well as in various solid solutions including $Ba_{1-x}Sr_xBO_3$ (B = Hf, Zr)[32,33] and $Sr_{1-x}A_xSnO_3$ (A = Ba, Ca)[17] where the $a^0b^-b^-$ tilt system is also observed but may parallel that seen in $CaTiO_3$.[3]

Variable Temperature Structures. The temperature dependence of the lattice parameters for Sr_2NiWO_6 was examined between room temperature and 500 °C (Figure 6). After we had collected these data, we became aware of a similar study by Gateshki et al.[20] The results of the two studies are generally in excellent agreement, with the present study finding slightly higher transition temperature $T_c \approx 375$ °C versus 315 °C. The tetragonal to cubic transition in Sr_2NiWO_6 has been reported several times with transition temperatures in the range 260−400 °C.[20,34] These differences

(32) Kennedy, B. J.; Howard, C. J.; Thorogood, G. J.; Hester, J. R. *J. Solid State Chem.* **2001**, *161*, 106.
(33) Li, L.; Kennedy, B. J.; Kubota, Y.; Kato, K.; Garrett, R. F. *J. Mater. Chem.* **2004**, *14*, 263−273.
(34) Tomaszewski, P. E. *Phase Transitions* **1992**, *38*, 127−220.

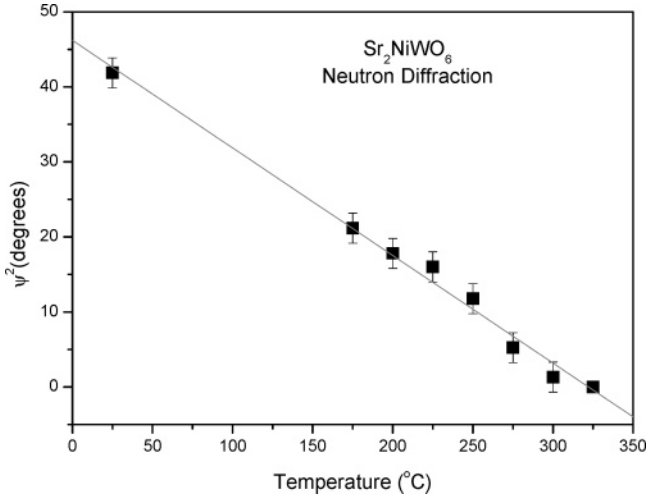

Figure 7. Temperature dependence of the square of the tilt angle in Sr_2NiWO_6. The angles were estimated from powder neutron diffraction data. The solid line is the linear fit to the data.

possibly arise from errors in temperature calibration and in the resolution of the diffraction data.[35] The temperature dependence of the volume does not show any indication of a discontinuity associated with the phase transition (Figure 6).

The nature of the transition can be established by examination of the temperature dependence of a suitable order parameter.[36] Since the *I*4/*m* structure arises as a consequence of tilting of the BO_6, octahedra we initially sought to use the tilt angle as a possible order parameter. To our initial surprise, we did not observe any systematic variation in the tilt angle over the entire temperature range studied. The problem is that the transition from $Fm\bar{3}m$ to *I*4/*m* in the rock-salt ordered double perovskites does not result in any additional superlattice reflections. Rather the tilting of the BO_6 octahedra simply alters the intensity of the *R*-point superlattice reflections that are, when X-ray methods are used, otherwise dominated by the difference in scattering of the two B-site cations. In an ideal situation it would be possible to accurately establish the atomic coordinates of the oxygen anions by suitable structural refinements; however, we found that refinements from powder X-ray data, gave poor precision in their values. X-ray methods provide a reasonable measure of the *M*−O distances; however, for tetragonal double perovskites in *I*4/*m*, we cannot experimentally determine the magnitude of the tilt using powder X-ray diffraction data alone. Neutron diffraction methods are expected to give better values for the oxygen coordinates and, hence, better estimates of the tilt angle. To verify this, we collected a small number of neutron diffraction patterns for Sr_2NiWO_6 between room temperature and 375 °C using the medium resolution diffractometer. Above 375 °C the sample reacted with the stainless steel holder. The tilt angle derived from the refined oxygen coordinates was observed to decrease from 6.5° at room temperature to near zero at 325 °C. A plot of φ^2 versus

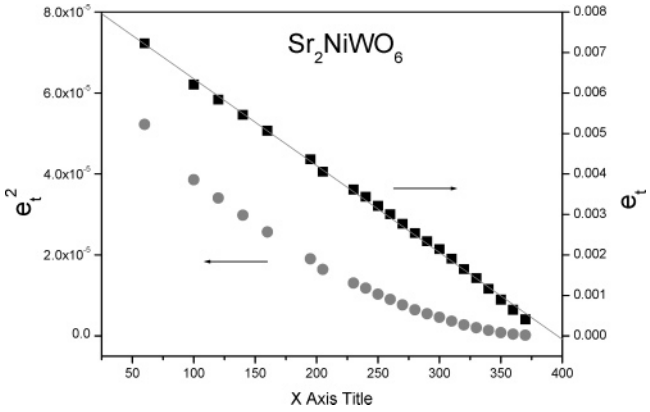

Figure 8. Temperature dependence of the tetragonal strain (squares) and square of the tetragonal strain (circles) in Sr_2NiWO_6. The solid line is the linear fit to the tetragonal strain.

temperature (Figure 7) was linear, indicative of a second-order transition at an estimated temperature 325 °C.

The nearly linear variation of the X-ray lattice parameters (Figure 6) can be taken as another indication of the second-order nature of the transition, and the transition temperature estimated from linear extrapolation of these parameters is a somewhat higher 397 °C. These results can be obtained more formally via spontaneous strains. The tetragonal strain (e_t) is given by[26]

$$e_t = \frac{2}{\sqrt{3}}\left(\frac{c - a\sqrt{2}}{a_0}\right) \approx 2\sqrt{3}\left(\frac{c - a\sqrt{2}}{c + 2a\sqrt{2}}\right)$$

where c and a are the lattice parameters in the tetragonal phase, and a_0 is the estimated value of the lattice parameter in the cubic structure were no transition to take place. A plot of the temperature dependence of this strain is linear (Figure 8). Since the strain is proportional to Q^2 (Q being the order parameter), it is inferred that the transition is continuous and second order in nature. The transition temperature is confirmed as 397 °C, somewhat higher than the temperature estimated from the loss of tetragonal distortion in the diffraction data (375 °C). This illustrates the problem of estimating the temperature of a continuous phase transition from diffraction data and highlights the value of extrapolation from parameters measured well away from the transition. A similar strategy can, of course, be used to estimate the critical composition for this tetragonal to cubic transition. Here we find a linear variation of strain on composition, the critical radius being estimated as r_A = 1.4817 Å corresponding to $Ba_{0.75}Sr_{1.25}NiWO_6$ in good agreement with the observed diffraction data.

We next sought to establish the nature of the monoclinic to tetragonal phase transition, through the study of $Ca_{0.6}Sr_{1.4}NiWO_6$. Initially data were collected from 100 to 800 °C in 25-deg intervals. The temperature dependence of the lattice parameters for this compound is shown in Figure 9. The lattice parameters show a clear discontinuity near 540 °C. To confirm that this is truly a first-order transition, a second series of measurements were made using finer temperature intervals (10°) over a limited temperature range of 450−650 °C. The results of the two studies are in excellent agreement. Figure 10 shows portions of the diffraction

(35) Yashima, M.; Mori, M.; Kamiyama, T.; Oikawa, K.; Hoshikawa, A.; Torii, S.; Saitoh, K.; Tsuda, K. *Chem. Phys. Lett.* **2003**, *375*, 240−246.
(36) Carpenter, M. A.; Becerro, A. I.; Seifert, F. *Am. Miner.* **2001**, *86*, 348−363.

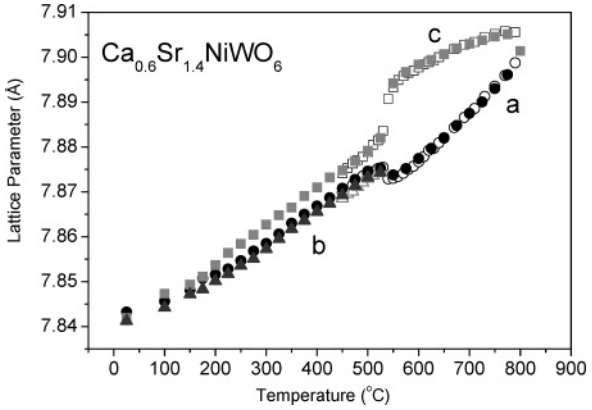

Figure 9. Variation of the reduced lattice parameters with temperature for $Ca_{0.6}Sr_{1.4}NiWO_6$. The open and closed symbols refer to two different experimental runs. The *a* and *b* values in the monoclinic and tetragonal cells have been multiplied by $\sqrt{2}$ for clarity.

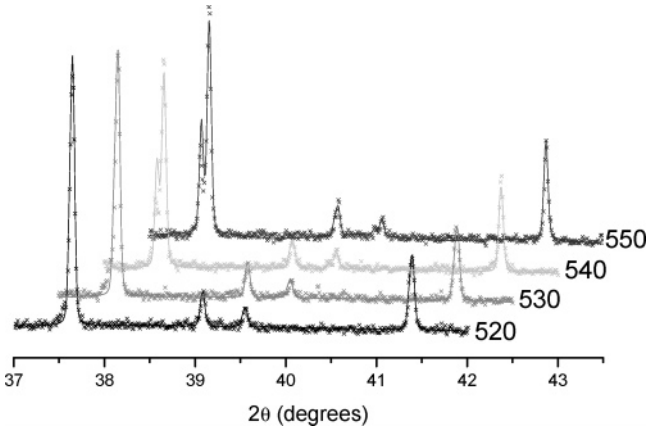

Figure 10. Portions of the observed and calculated powder X-ray diffraction profiles for $Ca_{0.6}Sr_{1.4}NiWO_6$. The patterns recorded at 520 and 530 °C were fitted in $P2_1/n$ and those at 540 and 550 °C were fitted in $I4/m$. Note the abrupt transition between the two structures between 530 and 540 °C.

patterns at four temperatures adjacent to the transition; 520 and 530 °C fitted in $P2_1/n$ and at 540 and 550 °C fitted in $I4/m$. As suggested by Figure 9, the structures at 520 and 530 °C are approximately tetragonal. Indeed, it was possible to fit the patterns assuming either $P2_1/n$ or $I4/m$, the former providing a better fit [$I4/m$: $a = 5.5696(2)$, $c = 7.8841(2)$ Å, $R_p = 6.58$, and R_{wp} 8.48%; $P2_1/n$: $a = 5.5702(2)$, $b = 5.5692(2)$, $c = 7.8855(1)$ Å, $\beta = 90.079(1)°$, $R_p = 6.24$, and R_{wp} 8.13%].

It is evident from Figure 9 that the structure of $Ca_{0.6}Sr_{1.4}NiWO_6$ remains tetragonal to 800 °C, the highest temperature available to us. Nevertheless it is possible to estimate the transition temperature by analysis of the tetragonal strain. The plot of strain versus temperature was not linear, as would be expected for a continuous second-order transition, but, as can be seen in Figure 11, the strain squared has a linear dependence on temperature. This suggests the transition to cubic in $Ca_{0.6}Sr_{1.4}NiWO_6$ is continuous but tricritical in nature. The linear fit to e_t^2 versus T indicates a critical temperature of around 820 °C. By contrast for Sr_2NiWO_6 the plot of e_t^2 versus T included in Figure 8 is clearly nonlinear.

Two other compositions were then studied: $Ca_{0.4}Sr_{1.6}NiWO_6$ and $Ca_{0.5}Sr_{1.5}NiWO_6$. For brevity, we only reproduce the results for the former composition here. In this oxide

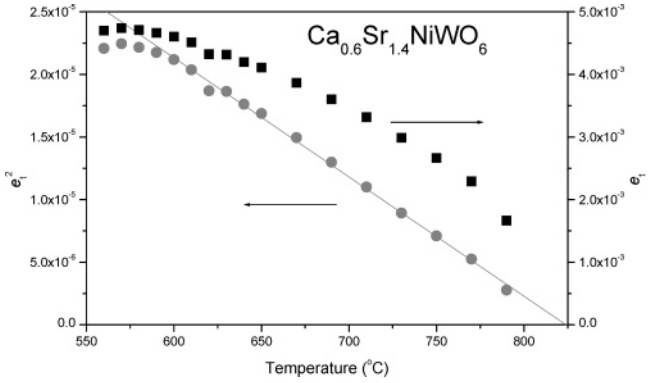

Figure 11. Temperature dependence of the tetragonal strain (squares) and square of the tetragonal strain (circles) in $Ca_{0.6}Sr_{1.4}NiWO_6$. The solid line is the linear fit to square of the strain. A deviation from linear behavior is observed below around 570 °C, that is in the region of the first-order $P2_1/n$ to $I4/m$ transition.

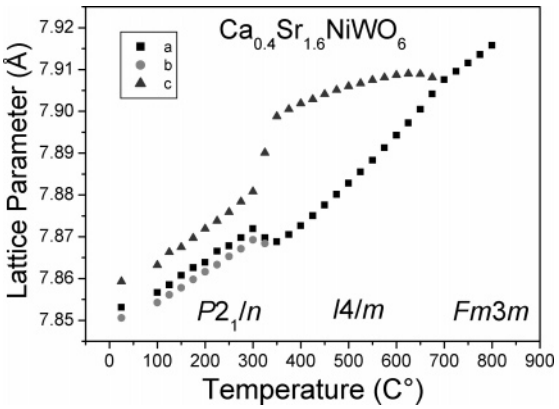

Figure 12. Temperature dependence of the reduced lattice parameters for $Ca_{0.4}Sr_{1.6}NiWO6$. The *a* and *b* values in the monoclinic and tetragonal cells have been multiplied by $\sqrt{2}$ for clarity.

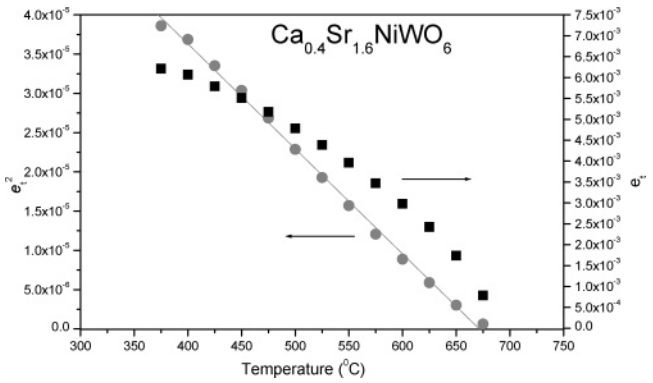

Figure 13. Temperature dependence of the tetragonal strain (squares) and square of the tetragonal strain (circles) in $Ca_{0.4}Sr_{1.6}NiWO_6$. The solid line is the linear fit to square of the strain.

we observe a strong first-order monoclinic to tetragonal transition near 320 °C and a continuous tetragonal to cubic transition near 700 °C. The temperature dependence of the tetragonal lattice parameters for this composition (Figure 12) resembles that for $Ca_{0.6}Sr_{1.4}NiWO_6$. The tetragonal strains are plotted in Figure 13. The transition to cubic at this composition is continuous and tricritical in nature.

From a thermodynamic viewpoint, the difference between second-order and tricritical arises from nonzero coefficients in the Landau free energy expansion. The equation has been given before, and the reader is referred to the work of Carpenter et al.[36] There are two possible physical reasons

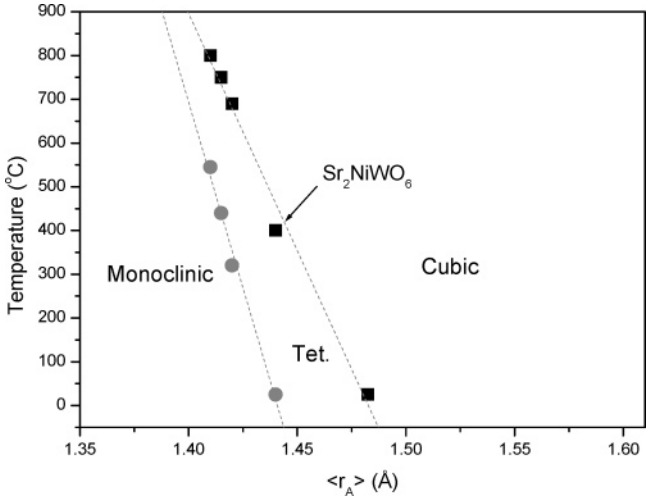

Figure 14. Phase diagram for the series A_2NiWO_6. The cubic structures are in $Fm\bar{3}m$ and the tetragonal structures are in $I4/m$.

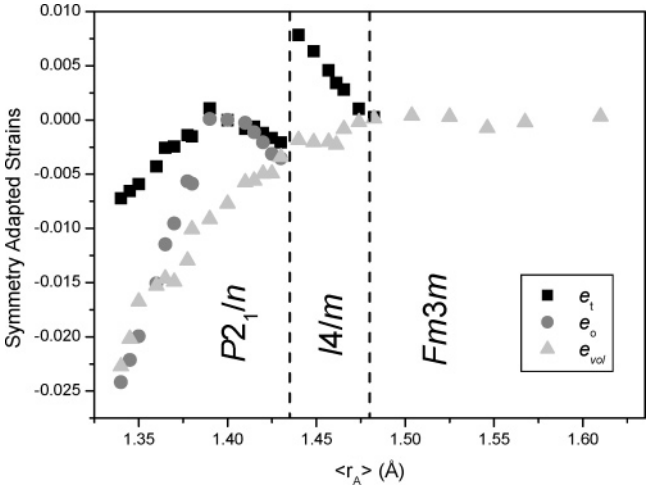

Figure 15. Composition dependence of the symmetry adapted strains in the series of oxides A_2NiWO_6. e_t is the tetragonal strain, e_o is the orthorhombic strain, and e_{vol} is the volume strain. The dashed vertical lines show the approximate points of the transitions.

for the tricritical nature of this transition in $Ca_{0.4}Sr_{1.6}NiWO_6$, as compared with the second-order nature of the transition in Sr_2NiWO_6. First the addition of Ca into the A-site is likely to result in a small amount of local Ca−Sr order in the structure (although the diffraction data suggests there is no long range order). An additional energy term is then required to drive the transition in the presence of this local order. Alternatively the tricritical nature of the transition may reflect the influence of a nearby third phase.

Although we are unaware of any studies showing a monoclinic to $I4/m$ transition in Sr_2NiWO_6 below room temperature it is likely that such a transition occurs. First the temperature for the $P2_1/n$ to $I4/m$ transition decreases rapidly with increasing Sr content, and second such a transition is observed in the closely related systems Sr_2CoWO_6 (T_c = 260 K)[20,29] and Sr_2ZnWO_6 (T_c = 60 °C).[20] Note that in both these cases the authors suggest there is a direct $I4/m - P2_1/n$ transition. The relationship between the effective size of the A-site cation, temperature, and symmetry is illustrated in Figure 14. The relatively small number of points notwithstanding it appears that the stability field for the tetragonal phase decreases as the size of the A-cation reduces, and it is possible that a direct monoclinic to cubic transition may occur in some situations. This has been observed in cryolite (Na_3AlF_6), which has Al and Na ordered in a double perovskite structure.[37]

On the Cubic Metric. As indicated above the volume composition plot shows evidence for considerable strain in the primitive monoclinic cell. It is possible to estimate spontaneous strains by extrapolation of the cell parameters from a fit to the cubic regions ($r_A > 1.48$) to all the samples. Neglecting the small monoclinic angle these strains are given by

$$e_1 = \frac{a\sqrt{2} - a_o}{a_0} \quad e_2 = \frac{b\sqrt{2} - a_o}{a_0}, \quad e_3 = \frac{c - a_o}{a_0}$$

The symmetry adapted strains are obtained from these components. The tetragonal strain is given by $e_t = 1/\sqrt{3}(2e_3 - e_1 - e_2)$, and its composition dependence is illustrated in Figure 15. A striking feature of this figure is the two linear regions for the tetragonal strain between $1.34 < r_A < 1.38$ and $1.44 < r_A < 1.48$ Å. The latter has already been referred to and describes the second-order tetragonal to cubic transition. The former is associated with the $P2_1/n$ to $I4/m$ transition and suggest a critical radius of around 1.41, corresponding to $Ca_{0.6}Sr_{1.4}NiWO_6$. The orthorhombic strain, given by $e_o = (e_1 - e_2)$, also varies linearly with composition in the region $1.34 < r_A < 1.40$ Å. An implication from these strains is that there may be a second transition near $r_A = 1.40$ Å. However, as discussed above, neutron diffraction measurements show no evidence for a second monoclinic phase. In the region $1.40 < r_A < 1.44$ Å, both the orthorhombic and tetragonal strains are very small. The form of Figure 15 is very similar to that of the spontaneous strains in the series $Ca_{1-x}Sr_xTiO_3$.[36] One is left with the intriguing situation that in both series there is a change in the strains that is not associated with a structural phase transition.

Conclusion

We have successfully prepared an extensive series of mixed Ni−W double perovskites of the type A_2NiWO_6 where A is a suitable combination of alkaline earth cations (Ca, Sr, or Ba). Using both synchrotron X-ray and neutron powder diffraction methods, we have demonstrated the following sequence of phases exists: $P2_1/n \xrightarrow{r_A = 1430\ \text{Å}} I4/m \xrightarrow{r_A = 1480\ \text{Å}} Fm\bar{3}m$ where the number refers to the effective ionic radii of the A-type cation. The former transition is first order. The same sequence of phases is observed in Sr_2CaWO_6,[38] and considering the tilt patterns, this sequence is similar to that seen in $Ca_{1-x}Sr_xTiO_3$.[39] While the variation in the lattice parameters and strains suggest a second monoclinic phase may exist, powder neutron diffraction measurements show this not to be the case.

(37) Zhou, Q. D.; Kennedy, B. J. *J. Solid State Chem.* **2004**, *177*, 654−659.

(38) Gateshki, M.; Igartua, J. M. *J. Phys.-Condens. Matter* **2004**, *16*, 6639−6649.

(39) Howard, C. J.; Withers, R. L.; Kennedy, B. J. *J. Solid State Chem.* **2001**, *160*, 8−12.

Variable temperature studies of selected samples were undertaken in addition to the composition-dependent studies. These demonstrate the $I4/m$ to $Fm\bar{3}m$ transition is continuous and second-order with respect to composition and with respect to temperature for Sr_2NiWO_6. This transition is continuous in the three Ca-doped samples studied as a function of temperature ($Sr_{2-x}Ca_xNiWO_6$; $x = 0.4, 0.5, 0.6$); however, in each of these samples the transition to the cubic phase is found to be tricritical. Where observed the temperature induced $P2_1/n$ to $I4/m$ transition is first-order as required by symmetry.

Acknowledgment. This work has been partially supported by the Australian Research Council. The work performed at the Australian National Beamline Facility was supported by the Australian Synchrotron Research Program, which is funded by the Commonwealth of Australia under the Major National Research Facilities program. The Australian Institute of Nuclear Science and Engineering supported the neutron diffraction experiments. The assistance of Dr. James Hester at the ANBF is gratefully acknowledged.

CM050900K